NANO LETTERS

Letter

pubs.acs.org/NanoLett

Multiplexed and Electrically Modulated Plasmon Laser Circuit

Ren-Min Ma,[†] Xiaobo Yin,[†] Rupert F. Oulton,[†] Volker J. Sorger,[†] and Xiang Zhang*[,†,‡]

[†]NSF Nanoscale Science and Engineering Center, 3112 Etcheverry Hall, University of California, Berkeley, California 94720, United States

[‡]Materials Sciences Division, Lawrence Berkeley National Laboratory, 1 Cyclotron Road, Berkeley, California 94720, United States

Supporting Information

ABSTRACT: With unprecedented ability to localize electromagnetic field in time and space, the nanometer scale laser promises exceptionally broad scientific and technological innovation. However, as the laser cavity becomes subwavelength, the diffraction of light prohibits the directional emission, so-called the directionality, one of the fundamental attributes of the laser. Here, we have demonstrated a deep subwavelength waveguide embedded (WEB) plasmon laser that directs more than 70% of its radiation into an embedded semiconductor nanobelt waveguide with dramatically enhanced radiation efficiency. The unique configuration of WEB plasmon laser naturally integrates photonic and electronic functionality allowing both efficient electrical modulation and wavelength multiplexing. We have demonstrated a plasmonic circuit integrating five independently modulated multicolored plasmon laser sources multiplexed onto a single semiconductor nanobelt waveguide, illustrating the potential of plasmon lasers for large scale, ultradense photonic integration.

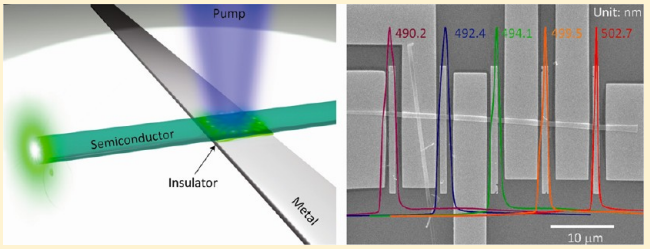

KEYWORDS: *Surface plasmon, laser, spaser, circuit, multiplexing and modulation*

Regarded as the key driver of ultradense optoelectronic circuitry, single-molecule sensing, ultrahigh-density data storage, nanoscale lasers have attracted much attention.[1−7] The research of nanoscale lasers is rapidly advancing, and a variety of approaches have been explored including Fabry−Pérot lasers,[8−10] whispering gallery lasers,[11−13] photonic crystal lasers,[14−17] and metallic lasers.[18−26] Recently, plasmon lasers with both a physical size and an optical mode confinement below the diffraction limit of light in a different number of dimensions have been demonstrated[19−21,24−26] using localized surface plasmons bound to metal surfaces.[27−31] With the unprecedented ability to generate intense electromagnetic radiation at the nanoscale in femtosecond time scales, plasmon lasers now stimulates the exploration of exceptionally broad scientific and technological innovation at the nanometer scale. However, critical challenges remain and must be tackled before these plasmon lasers can be utilized as integrated light sources. First, the large momentum mismatch of light inside and outside of a deep subwavelength plasmon cavity results in diffraction into all directions, inhibiting directional emission and efficient collection of optical power from a plasmon laser for practical applications. Furthermore, due to the intrinsic metal Ohmic loss limited quality factor, the radiation efficiency of plasmon laser is very low. The devices deliver energy to the nanoscale plasmonic mode but just release only a small part of their optical energy to the far field before it is dissipated in the metal. Last, scaling down integrated photonics requires multiplexed nanolasers with direct on-chip electrical modulation, which places constraints on the integration of driving electronics without disturbing the cavity mode or increasing the device footprint.

Here, we demonstrate an integrated waveguide embedded (WEB) plasmon laser that efficiently converts surface plasmons into directional laser emission by launching more than 70% of its radiation into a semiconductor nanobelt waveguide. Due to this efficient conversion, the radiation efficiency of the plasmon laser has been enhanced about 20 times to 35%. We show an array of five WEB lasers with different colors multiplexed onto a single semiconductor waveguide. Each of these plasmon lasers has a submicrometer footprint and operates at room temperature. Moreover, this unique design naturally integrates electronic and photonic elements, enabling independent direct electrical modulation of each plasmon laser. A maximum modulation depth of 11 dB for merely 1 V of bias sweep is obtained. These unique properties demonstrate an intriguing hybrid photonic and plasmonic circuit that integrates multicolor nanoscopic plasmon lasers with direct electrical modulation and wavelength multiplexing onto a single photonic semiconductor waveguide.

The WEB plasmon laser is constructed by crossing a semiconductor cadmium sulfide (CdS) nanobelt waveguide over a silver strip with a 5-nm-thick magnesium fluoride (MgF_2) gap layer. At the semiconductor−metal intersection, the surface plasmon effect induces a high effective refractive

Received: July 29, 2012
Revised: September 2, 2012
Published: September 18, 2012

index, forming a square-shaped plasmon laser cavity. The dominant radiative loss of the cavity is scattering into the semiconductor waveguide that guides the majority of the laser radiation into desired directions (Figure 1a). A CdS nanobelt[32] with high luminescence quantum efficiency serves as both gain medium in the laser cavity and semiconductor waveguide

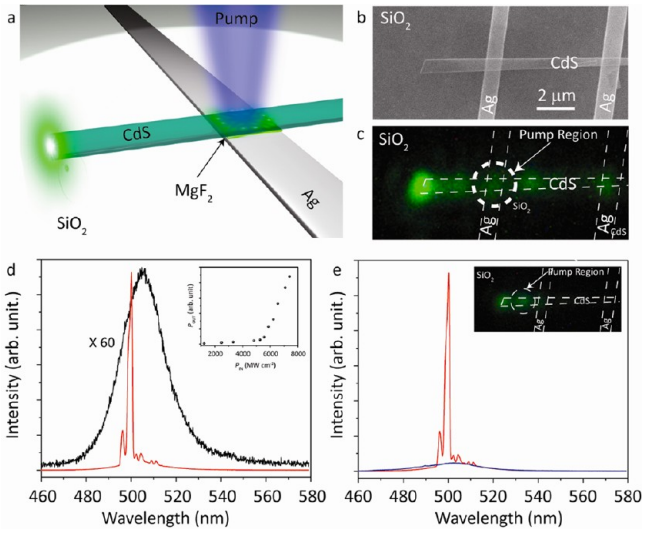

Figure 1. Waveguide embedded (WEB) plasmon laser with directional emission. (a) Schematic of a WEB plasmon laser optically pumped. Only the cavity region is pumped and laser emission is launched to the semiconductor waveguide, which scatters into free space from its end facet. (b–c) the SEM micrograph (b) and CCD-camera imaged lasing (c) of a 620 nm wide, 100 nm thick CdS nanobelt crossing a 250 nm thick, 790 nm wide silver strip separated by a 5 nm MgF_2 gap. While only the crossing region is excited (white dashed circle in c), the brightest light spot appears at the CdS waveguide end facet. Scattering lights from the laser cavity and three other locations is considerably weaker. The obtained laser emission-to-waveguide coupling efficiently is about 80%. (d) The increased coherence of collected spectra from all scattered light areas with increasing pump power indicates the occurrence of laser action. The transition from spontaneous emission (3.3 GW cm^{-2}, black) to full laser oscillation (7.4 GW cm^{-2}, red) is clearly visible by both the significant line width narrowing effect and the clear threshold behavior in integrated light output versus pump response (inset). (e) Control experiment where the CdS nanobelt is excited away from the crossed region at a pump power of 7.4 GW cm^{-2}. The obtained spectrum indicates that it is a broad band-edge spontaneous emission of CdS with full width at half-maximum of about 18 nm (blue curve, emission pattern shown in the inset), which is dramatically in contrast with the high purity and intense plasmon lasing emission from the crossed plasmonic cavity region with full width at half-maximum under 2 nm at the same power (red curve, emission pattern shown in panel c). This is an unambiguous evidence that the crossed metal strip and semiconductor waveguide can form a high quality plasmonic cavity which can lase under pump with threshold much lower than that of the Fabry–Perot photonic cavity mode of CdS waveguide with a width of just hundreds of nanometer alone.

outside for emitted laser light. The 5-nm MgF_2 gap layer is used to pull the electric field into the gap region thus confining the plasmonic mode significantly below the diffraction limit of light with relatively low metal Ohmic loss.[33] Figure 1b shows the SEM micrograph of a WEB plasmon laser. The footprint of the plasmon laser is about 0.48 μm^2. The directional emission of the laser is observed by optically pumping the cavity region and imaging the scattered light (Figure 1c). At pump intensities above the laser threshold, the brightest light spot appears at the end facet of the semiconductor waveguide instead of at the excited plasmon laser cavity region, indicating that laser emission is efficiently coupled into the waveguide. The transition from spontaneous emission to full laser oscillation is clearly visible by both the rapid increase in spectral purity of the plasmon cavity modes (line width narrowing effect) and the clear threshold behavior in integrated light output versus pump response (Figure 1d). It is worth noting that the current threshold can be reduced dramatically by using a laser with longer pulse, since the pump laser pulse width (~100 fs) we used now is just about 1/1000th of the spontaneous emission lifetime. The observed lasing signal at the end of the waveguide originates from the *plasmonic* cavity mode at the intersection, but is guided to the waveguide facet by the *photonic* waveguide mode supported in the semiconductor strip waveguide. The efficient conversion of amplified surface plasmons to the directional waveguide emission is evident from the optical image of a lasing device shown in Figure 1c. Integrating the intensity of all emitted light, we estimate that 80% of the light emission is coupled to the waveguide propagating in both directions away from the laser due to the symmetry of the structure.

It is important to emphasize that the observed plasmon lasing behavior solely originates from the WEB plasmon cavity mode in the intersection region. Figure 1e shows a control experiment where the CdS nanobelt is locally excited away from the crossed region at a pump power of 7.4 GW cm^{-2}. The obtained spectrum indicates that it is a broad band-edge spontaneous emission of CdS with full width at half-maximum of about 18 nm (Figure 1e blue curve), which is dramatically in contrast with the high purity and intense plasmon lasing emission from the WEB plasmon cavity region with full width at half-maximum under 2 nm at the same pump power (Figure 1e red curve, the same as the red curve in Figure 1d). This is an unambiguous evidence that the crossed metal strip and semiconductor waveguide have formed a high quality WEB plasmon laser cavity. The Fabry–Perot mode across the width of CdS nanobelt has radiation loss (estimated to be about 4×10^4 cm^{-1}) even much higher than the metal Ohmic loss due to the small dimensions of width (~620 nm) and thickness (~100 nm) which prevents the lasing from the photonic CdS nanobelt.

The experimental observation of efficient directional waveguide coupling from a WEB plasmon laser into a semiconductor waveguide is supported by full wave electromagnetic simulations (Figures 2 and 3). The relative momentum and spatial intensity profiles determine the coupling strength between the plasmon cavity mode and the external modes. Figure 2 shows the mode matching conditions of the WEB plasmon laser cavity. The effective refractive indexes of all the involved modes are plotted in Figure 2a. The effective refractive index of the plasmonic TM mode with dominant electric field perpendicular to the substrate surface at the intersection region is much higher than that of the modes of pure semiconductor nanobelt and metal strip alone, which is the key to form a high quality plasmon cavity in the crossed region (Figure 2a). Figure 2b–d shows the mode profiles along the direction perpendicular to the metal surface of the semiconductor–insulator–metal gap surface plasmon mode, semiconductor nanobelt waveguide mode and surface plasmon mode at the Ag–air interface. The thickness of the CdS nanobelt is 100 nm in the simulation of Figure 2b–d. We can see that the TE mode

dx.doi.org/10.1021/nl302809a | *Nano Lett.* 2012, 12, 5396–5402

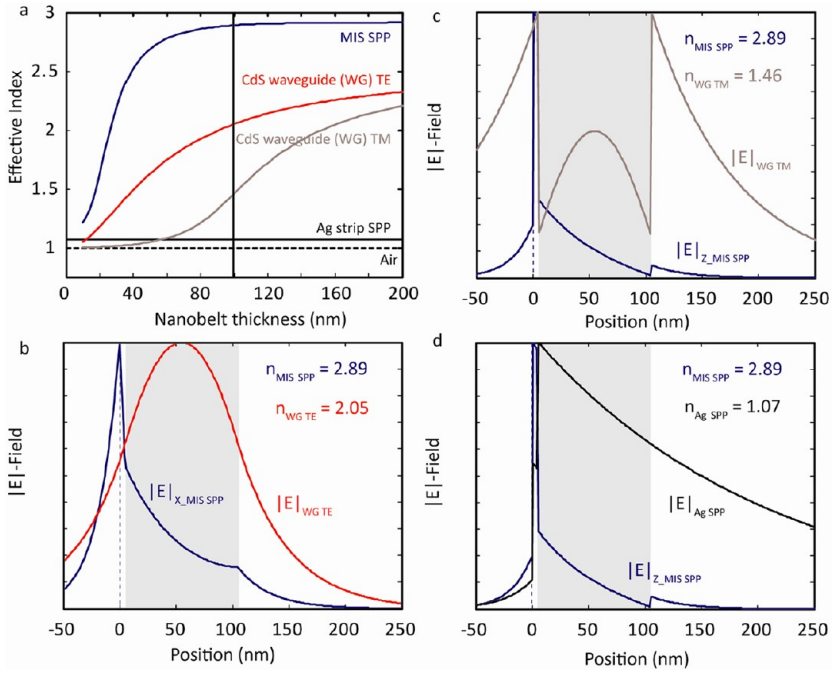

Figure 2. Mode matching conditions of the WEB plasmon laser. (a) The effective indexes of the semiconductor−insulator−metal gap surface plasmon mode, semiconductor nanobelt waveguide mode, surface plasmon mode at the Ag−air interface, and air. In the plotted region, the TE mode of the semiconductor waveguide is the most confined mode with the highest momentum available outside of the intersection region. (b−d) Mode profiles along the direction perpendicular to the metal surface of the semiconductor−insulator−metal gap surface plasmon mode, semiconductor nanobelt waveguide mode, and surface plasmon mode at the Ag−air interface. The dominant electric field of the gap surface plasmon mode is E_z. The E_x and E_y components of this mode share similar profiles. TE mode of the semiconductor waveguide is with the best spatial mode matching with the weaker in-plane electric fields (E_x and E_y) of the WEB plasmon cavity mode. The thickness of the CdS nanobelt is 100 nm in simulations.

of the semiconductor waveguide is the most confined mode available with both the best momentum and spatial mode matching with the weaker in-plane electric fields (E_x and E_y) of the WEB plasmon cavity mode. Although TM modes of the semiconductor waveguide and silver strip share the same dominant E_z electric field component in the cavity, they are delocalized and low momentum leading to both poor momentum and spatial mode matching to the cavity mode. While the weak coupling to all available modes ensures relatively large cavity quality factors, the best momentum and spatial mode matching is achieved for the TE semiconductor waveguide mode leading to the observed preferential coupling to the semiconductor waveguide.

The coupling between the WEB plasmon cavity and varies radiation channels is further studied by three-dimensional electromagnetic simulation (Figure 3). We can see that there is a square-shaped plasmon cavity[25] formed in the intersection region due to the high effective index contrast between the surface plasmon mode and the surroundings (Figure 3a). The dominant electric field, E_z, is confined well in the intersection region (Figure 3g). The in-plane fields, E_x and E_y, can be efficiently coupled to the TE mode of the semiconductor waveguide which is the most confined mode available with both the best momentum and spatial mode matching them (Figure 3h−i). The observed significantly preferential light capture and subsequent guiding by the semiconductor waveguide suggests that mode coupling is stronger between this photonic waveguide and plasmon cavity modes (Figure 3a−b,d). Significantly, our calculations show that more than 70% of all of the radiated energy from the laser cavity is efficiently coupled to the waveguide with thickness above 60 nm, and about 5% of the energy is coupled to plasmonic modes of the silver strip. A higher efficiency is measured from the scattered light in the aforementioned WEB laser (Figure 1c) where the energy coupled to the plasmonic modes is not taken into account. When the CdS strip is thinner than 60 nm, the cavity still maintains a similar quality factor due to the plasmonic confinement effect; however, the coupling efficiency to the semiconductor waveguide reduces due to the decreased effective index and the cutoff of photonic waveguide modes. For such thin waveguides, the light scattered to free space increases, and the dominant waveguide coupling channel switches to the metal strip, whose surface plasmon mode has the better momentum and spatial mode matching to the WEB plasmon cavity. In this way, WEB plasmon lasers may serve as coherent surface plasmon sources for constructing nanoplasmonic circuits based entirely on surface plasmons.

The unique architecture of the WEB plasmon laser allows for implementing multicolor laser arrays and multiplexing them into the same waveguide. With each laser occupying a footprint less than a square micrometer, we demonstrate a five-channel single-mode WEB plasmon laser array multiplexed onto a single semiconductor waveguide by integrating a semiconductor strip onto multiple silver strips fabricated by E-beam lithography (Figure 4a). As shown in Figure 4b, each laser emits a different color because the varied width of the waveguide tunes the resonant condition of plasmon cavity and therefore the emission wavelength. The full width at half-maximum of a single mode plasmon laser emission can be narrower than 1 nm (Figure 4b). Since the propagating mode in the semiconductor waveguide is the TE mode with electric field parallel to the substrate surface, which interacts very weakly with both the material discontinuities and the modes of neighboring WEB plasmon cavities. As a result, the emission from each laser

dx.doi.org/10.1021/nl302809a | *Nano Lett.* 2012, 12, 5396−5402

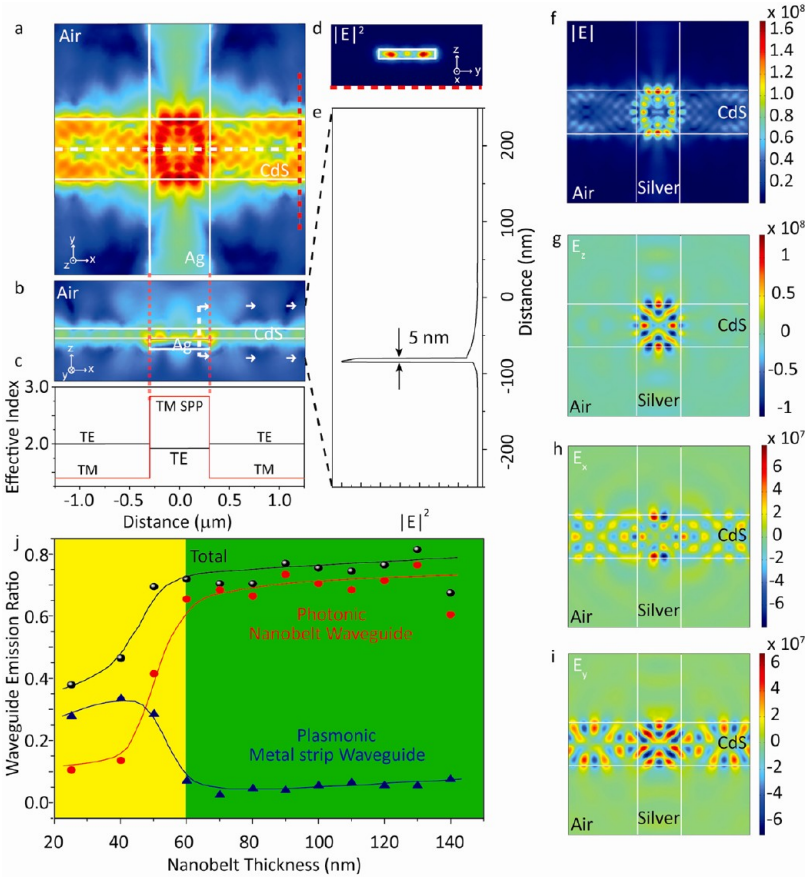

Figure 3. 3D electromagnetic simulation of a WEB plasmon laser and the laser-to-waveguide coupling efficiency. (a) Electric field intensity distribution viewed from above CdS strip (profiled by two horizontal white lines) crossing Ag strip (profiled by two vertical white lines; both 600 nm in width and 100 nm in thickness) in log scale separated by a 5 nm MgF_2 gap. The surface plasmon effect creates a local laser cavity in the cross region (the square area profiled by white lines in the middle of figure) by total internal surface plasmon reflection. The cavity's radiative losses are predominately launched into the same CdS waveguide directly. (b) Electric field intensity distribution cross section in log scale in the $x-z$ plane along the white dashed line in a. (c) Effective indices of TE and TM modes in cross region and in CdS strip region along the white dashed line in a. (d) Electric field intensity ($|E|^2$) distribution cross section along the red dashed line in a (the mode profile of out coupled light in CdS waveguide), indicating that the field is well-confined in the waveguide away from cavity region. (e) Electric field intensity ($|E|^2$) distribution along the white dashed line in b (the field distribution along the z-axis in intersection cavity region), indicating that the field is well-confined in the 5 nm low permittivity gap region. (f–i) The electric field intensity distributions of $|E|$, E_z, E_x, and E_y in the middle of CdS viewed normal to the sample substrate in linear scale. The dominant electric field, E_z, is confined well in the intersection region (g). The in-plane fields, E_x and E_y, are efficiently coupled to the TE mode of the semiconductor waveguide which is the most confined mode available with both the best momentum and spatial mode matching them (h–i). (j) Approaching 80% of all radiated energy of the plasmon cavity with a 600-nm-by-600-nm in plane size can be coupled to the waveguide for thicknesses greater than 60 nm (green region). Below about 60 nm (yellow region), the main coupling channel is changing to the metal strip waveguide, where the WEB plasmon lasers serve as sources of coherent surface plasmons.

device can be effectively transmitted across neighboring cavities, without significant scattering or interference, which allows the embedded waveguide to effectively multiplex the emission of all WEB plasmon lasers. We note that the number of lasing modes can be tuned by the thickness of a CdS strip. The single mode operation occurs here because that a thicker CdS strip intersecting a metal strip induced plasmon cavity has a weak effective index contrast with CdS nanobelt waveguiding modes and thus supports less square cavity modes. All of the lasing behaviors have been verified by two measures:[34] (1) There are clear linear–superlinear–linear transitions in the pump intensity dependence of the total output power curves of all measured lasing devices; (2) The obtained intensity of lasing cavity mode peaks exceed the spontaneous emission background by at least 1 order of magnitude. The spectra evolution, threshold, and line width narrowing behaviors of the WEB plasmon laser labeled as 5 in Figure 4a have been shown in Figure 4c. Others are supplied in the Supporting Information. We have observed a dramatic line width narrowing from about 20 nm to lower than 1 nm around the threshold indicating the onset of lasing. With increasing pump power well above threshold, the spectrum becomes asymmetry, and the line width slightly broadens. For the large conventional cavity lasers under continuous wave excitation, the line width will decrease inversely with the pump power above threshold due to an increasing degree of population inversion, that is, the usual Schawlow–Townes behavior. However, for micro and nanoscale lasers under fast pulsed excitation, the stimulated emission rate can become comparable to phonon relaxation rate that induces electronic nonequilibrium of the gain in the lasing regime. The resulting nonequilibrium energy distribution of carriers gives the broadening and asymmetry of the lasing peak.[35–39]

dx.doi.org/10.1021/nl302809a | *Nano Lett.* 2012, 12, 5396–5402

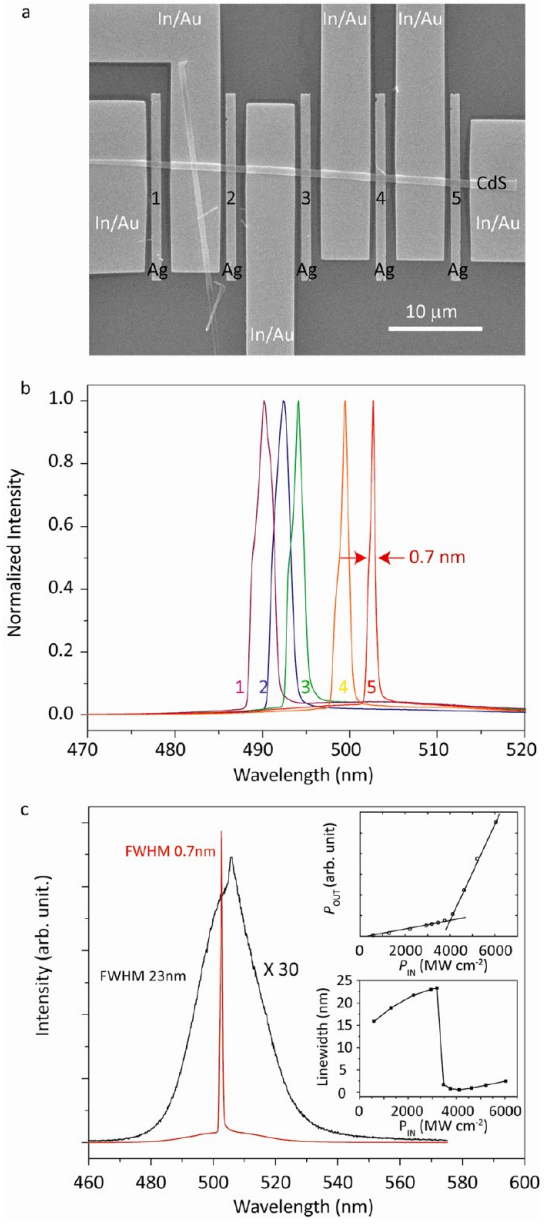

Figure 4. A multiplexed array of WEB plasmon lasers. (a) WEB plasmon lasers are straightforward to be assembled into integrated arrays. Here, five WEB plasmon laser devices are assembled from the same CdS strip crossing five silver strips with widths of 1 μm. For electrical interface, In/Au (10/120 nm) ohmic contact electrodes are defined through lithography and lift-off processes. (b) Spectra of these five WEB plasmon laser covering a 12 nm range. Such a realization of multicolor-array emission into a single waveguide is a promising step toward on-chip wavelength-division-multiplexing. (c) The spectra evolution, threshold, and line width narrowing behaviors of the WEB plasmon laser labeled as 5 in panel a. Others are shown in the Supporting Information. The transition from spontaneous emission (2.9 GW cm^{-2}, black) to full laser oscillation (4.6 GW cm^{-2}, red) is clearly visible by both the rapid increase in spectral purity of the cavity modes, the clear threshold behavior in integrated light output versus pump response (inset, top) and the rapidly narrowing of line width (inset, bottom).

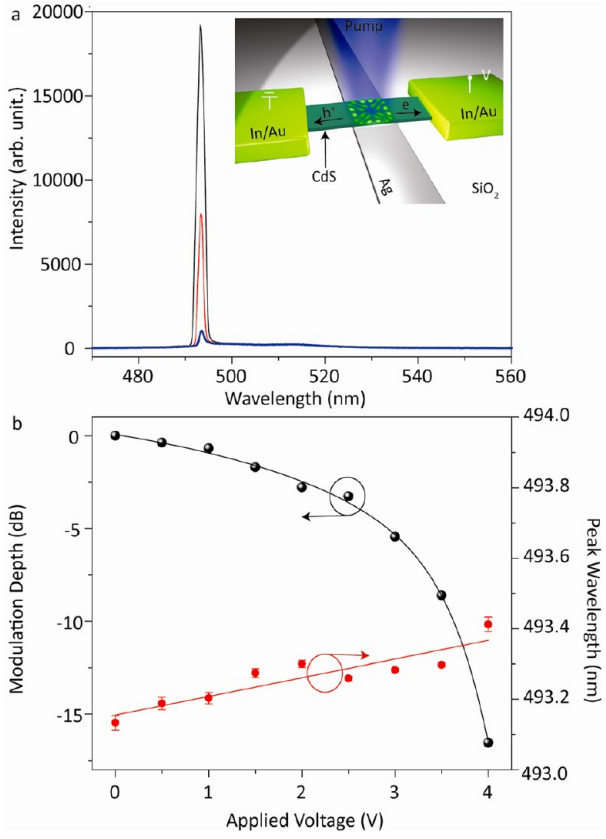

Figure 5. Direct electrical modulation of WEB plasmon laser. The carrier concentration in the WEB plasmon cavity can be tuned via an applied bias on two electrodes placed onto the CdS nanobelt. For electrical modulation test, In/Au (10/120 nm) ohmic contact electrodes are defined through lithography and lift-off processes. (a) Laser spectra of the device under a peak pump intensity of 3.8 GW cm^{-2} under various applied bias for a 1.15 um width, 140 nm thick CdS strip crossing 250 nm thick, 1 μm width silver strip separated by a 5 nm MgF_2 gap. Black line, 2.5 V; Red line, 3.5 V; Blue line, 4.0 V. Inset: Schematic of the direct electrical modulated WEB plasmon laser. (b) The lasing peak intensity of the device shows a 16 dB modulation depth within a 4 bias change, while the peak wavelength shift is below 0.3 nm over the entire bias region owing to the free carrier plasma effect.

The metal and semiconductor strips forming the plasmon laser cavity not only can serve as out-coupling waveguides but also can be used as electrical contacts simultaneously, allowing carriers to be transported into and out-of the cavity free from jeopardizing the well-confined plasmon modes at all. We have employed this unique property to enable direct laser amplitude modulation here, while the opposite operation, injecting electrons and holes into the active cavity region, can lead to an electrically pumped semiconductor plasmon laser. As shown in the inset of Figure 5, we integrate two In/Au electrodes at both ends of the waveguide to demonstrate modulation of the laser intensity by extracting electron–hole pairs from the cavity region by biasing the two electrodes (Figure 5a). Remarkably, the laser peak intensity can be modulated by 16 dB for a peak bias of 4 V by tuning the electron–hole pair concentration in CdS and thus the total gain of the laser (Figure 5b). A maximum modulation strength of 11 dBV^{-1} is experimentally demonstrated. Since the applied bias changes the density of excited carriers in the cavity, the real part of the refractive index of CdS is also changed due to the plasma dispersion effect.[40] As a result, a linear shift of peak emission wavelength is expected as shown in Figure 5b. We estimate that the carrier density in a lasing WEB plasmon cavity changes by about 4.4 × 10^{18} cm^{-3} for a voltage sweep of 4 V (see the Supporting Information). It

dx.doi.org/10.1021/nl302809a | Nano Lett. 2012, 12, 5396–5402

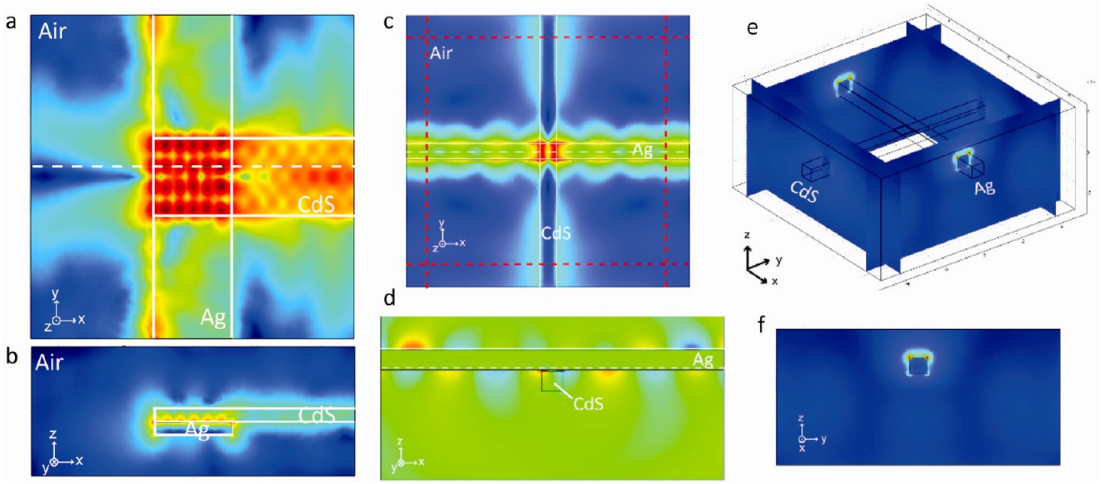

Figure 6. Unidirectional emission and scaling down of WEB plasmon laser. (a–b) Unidirectional emitted WEB plasmon laser. (a) Electric field intensity distribution viewed from above CdS nanobelt crossing Ag strip (both 600 nm in width and 100 nm in thickness) in log scale separated by 5 nm MgF_2 gap. The cavity's radiative emission are predominately launched into the right side CdS waveguide directly, since the left side waveguide is cut off which makes the corresponding out coupling boundary to be total internal reflective. (b) Electric field intensity distribution cross section in log scale in x–z plane along the white dashed line in a. (c–f) 3D electromagnetic simulation of a WEB plasmon laser constructed on CdS and Ag waveguide with lateral dimensions for 60 nm (thickness) × 60 nm (width). (c) Electric field intensity distribution viewed from above CdS nanobelt crossing Ag strip separated by 5 nm MgF_2 gap in log scale. (d) Electric field intensity distribution cross section in log scale in the x–z plane along the white dashed line in a. (e) Electric field |E| distribution cross section along the red dashed line in a, indicating that the major emission from the cavity is captured and guided by the subdiffraction Ag surface plasmon waveguide. (f) Electric field |E| distribution cross section along one red dashed line on Ag in c, indicating the mode profile of out coupled light in Ag surface plasmon waveguide.

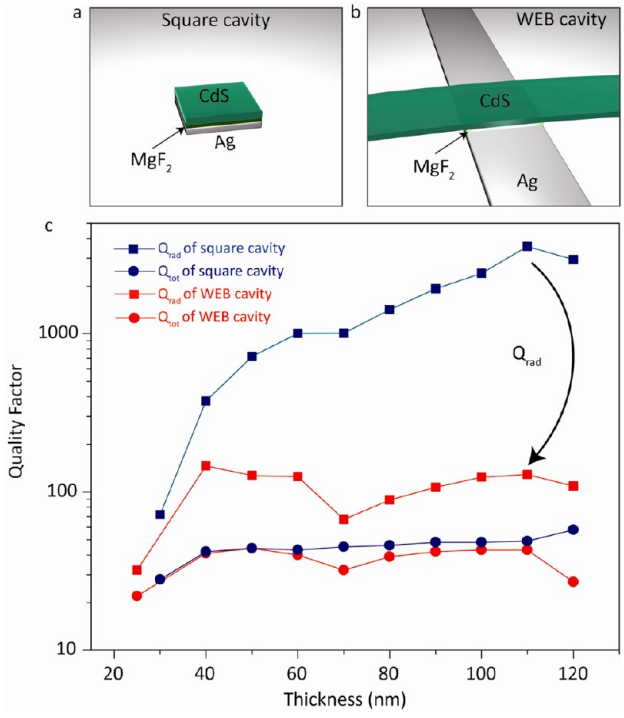

Figure 7. Radiation efficiency enhancement of WEB plasmon laser. The extracted total and radiative quality factors of square cavities and WEB plasmon cavities through 3D electromagnetic simulation. (a–b) Schematic images of a square cavity (a) and a WEB cavity (b). (c) Calculated total and radiative quality factors of square cavities and WEB cavities for varies CdS strip thickness. The radiative efficiency of the cross cavity is about 35% estimated by the radiative quality factor relative to the quality factor of the cavity. While the estimated radiative efficiency is just about 2% for the square cavity due to a high radiative Q.

is remarkable that this value is of the same order as the inversion density needed in bulk CdS laser despite the much higher loss of a plasmon cavity.[41] This is mainly due to the much higher spontaneous emission β factor, spatial gain overlap factor, and Purcell factor of deeply confined plasmon cavity modes compared to that of diffraction limited cavity modes.[18,20,21,42]

The WEB plasmon laser can also achieve unidirectional out coupling by cutting off one out coupling waveguide. Providing the cut is made at the silver nanowire edge, the corresponding cavity boundary would become total internal reflective. Figure 6a–b shows a simulation indicating the excellent unidirectional coupling possible. We note that further scaling down the waveguide size is also possible, where the fundamental dipole resonant mode will preferentially couple to metal strip surface plasmon waveguide. We have examined a CdS waveguide with lateral dimensions for 60 nm × 60 nm and a Ag waveguide with lateral dimensions for 60 nm × 60 nm with a three-dimensional electromagnetic simulation. We find a fundamental dipole mode cavity formed in the cross region and the major emission from the cavity is captured and guided by the subdiffraction Ag surface plasmon waveguide (Figure 6c–f).

In a plasmon cavity, the total quality factor is usually limited by the metal Ohmic loss. Thus, the devices deliver energy to the nanoscale plasmonic mode but just release only a small part of their optical energy to the far field before it is dissipated in the metal.[6] Since the fraction of energy radiating out of the cavity depends on the radiative quality factor relative to the quality factor of the cavity, reducing the radiation quality factor to a certain level can increase the radiation (energy) efficiency of a plasmon laser, while still maintain mediate total quality factor. In the WEB plasmon laser, due to the efficient conversion of surface plasmons in the WEB plasmon cavity to photons propagating in photonic waveguide, the radiation quality factor can be reduced by more than 1 order of

dx.doi.org/10.1021/nl302809a | Nano Lett. 2012, 12, 5396–5402

magnitude comparing to the plasmon square cavity as shown in Figure 7. The radiative efficiency of the cross cavity is about 35% estimated by the radiative quality factor relative to the quality factor of the cavity, while the estimated radiative efficiency is just about 2% for the square cavity due to a high radiative quality factor. The crossing waveguide configuration has significantly enhanced the percentage of energy coupled out of the plasmon laser.

In summary, we have demonstrated a directionally emitting WEB plasmon laser that efficiently converts coherent surface plasmons from a small laser cavity into an embedded photonic semiconductor waveguide. The WEB plasmon laser has an enhanced radiation efficiency of about 35%. Effective electrical modulation and wavelength multiplexing of WEB plasmon lasers at room temperature have been demonstrated experimentally. The hybrid photonic and plasmonic circuit integrates four key functions including: multicolored plasmon light sources, direct electrical modulation, efficient waveguide collection and out-coupling, and wavelength multiplexing in a compact and novel configuration, paving the way toward large scale on-chip integrated hybrid optoelectronic circuitry.

■ ASSOCIATED CONTENT

Supporting Information

(1) Device fabrication and experiment setup; (2) numerical mode simulations; (3) detailed spectral and light-pump response of WEB laser array; (4) carrier density modulation in lasing WEB plasmon laser. This material is available free of charge via the Internet at http://pubs.acs.org.

■ AUTHOR INFORMATION

Corresponding Author

*E-mail: xiang@berkeley.edu.

Notes

The authors declare no competing financial interest.

■ ACKNOWLEDGMENTS

We acknowledge financial support from the U.S. Air Force Office of Scientific Research (AFOSR) under Grant No. FA9550-12-1-0197.

■ REFERENCES

(1) Bergman, D. J.; Stockman, M. I. *Phys. Rev. Lett.* **2003**, *90*, 027402.
(2) Garcia-Vidal, F. J.; Moreno, E. *Nature* **2009**, *461*, 604−605.
(3) Miller, D. A. B. *Proc. IEEE* **2009**, *97*, 1166−1185.
(4) Brongersma, M. L.; Shalaev, V. M. *Science* **2010**, *328*, 440−441.
(5) Berini, P.; Leon, I. D. *Nat. Photonics* **2012**, *6*, 16−24.
(6) Ma, R.-M.; Oulton, R. F.; Sorger, V. J.; Zhang, X. *Laser Photonics Rev.* **2012**, DOI: 10.1002/lpor.20110004.
(7) Ding, K.; Ning, C. Z. *Light: Sci. Appl.* **2012**, DOI: 10.1038/lsa.2012.20.
(8) Huang, M. H.; et al. *Science* **2001**, *292*, 1897−1899.
(9) Duan, X.; Huang, Y.; Agarwal, R.; Lieber, C. M. *Nature* **2003**, *421*, 241−245.
(10) Gather, M. C.; Yun, S. H. *Nat. Photonics* **2011**, *5*, 406−410.
(11) Zhang, Z.; Yang, L.; Liu, V.; Hong, T.; Vahala, K.; Scherer, A. *Appl. Phys. Lett.* **2007**, *91*, 111119.
(12) Song, Q.; Cao, H.; Ho, S. T.; Solomon, G. S. *Appl. Phys. Lett.* **2009**, *94*, 061109.
(13) Chen, R.; et al. *Nat. Photonics* **2011**, *5*, 170−175.
(14) Park, H.-G.; et al. *Science* **2004**, *305*, 1444−1447.
(15) Strauf, S.; et al. *Phys. Rev. Lett.* **2006**, *96*, 127404.
(16) Ellis, B.; et al. *Nat. Photonics* **2011**, *5*, 297−300.
(17) Noda, S. *J. Opt. Soc. Am. B* **2010**, *27*, B1−B8.
(18) Hill, M. T.; et al. *Nat. Photonics* **2007**, *1*, 589−594.
(19) Noginov, M. A.; et al. *Nature* **2009**, *460*, 1110−1113.
(20) Oulton, R. F.; et al. *Nature* **2009**, *461*, 629−632.
(21) Hill, M. T.; et al. *Optics Express* **2009**, *17*, 11107−11112.
(22) Nezhad, M. P.; et al. *Nat. Photonics* **2010**, *4*, 395−399.
(23) Yu, K.; Lakhani, A.; Wu, M. C. *Opt. Express* **2010**, *18*, 8790−8799.
(24) Kwon, S.-H.; et al. *Nano Lett.* **2010**, *10*, 3679−3683.
(25) Ma, R.-M.; Oulton, R. F.; Sorger, V. J.; Bartal, G.; Zhang, X. *Nat. Mater.* **2011**, *10*, 110−113.
(26) Khajavikhan, M.; et al. *Nature* **2012**, *482*, 204−207.
(27) Maier, S. A.; et al. *Nat. Mater.* **2003**, *2*, 229−232.
(28) Barnes, W. L.; Dereux, A.; Ebbsen, T. W. *Nature* **2003**, *424*, 824−830.
(29) MacDonald, K. F.; Samson, Z. L.; Stockman, M. I.; Zheludev, N. I. *Nat. Photonics* **2009**, *3*, 55−58.
(30) Gramotnev, D. K.; Bozhevolnyi, S. I. *Nat. Photonics* **2010**, *4*, 83−91.
(31) Cai, W.; Shin, W.; Fan, S.; Brongersma, M. L. *Adv. Mater.* **2010**, *22*, 5120−5124.
(32) Ma, R.-M.; Dai, L.; Qin, G.-G. *Nano Lett.* **2007**, *7*, 868−873.
(33) Oulton, R. F.; Sorger, V. J.; Genov, D. A.; Pile, D. F. P.; Zhang, X. *Nat. Photonics* **2008**, *2*, 496−500.
(34) Zimmler, M. A.; Bao, J.; Capasso, F.; Müller, S.; Ronning, C. *Appl. Phys. Lett.* **2008**, *93*, 051101.
(35) Jahnke, F.; Koch, S. W. *Opt. Lett.* **1993**, *18*, 1438.
(36) Mohideen, U.; Slusher, R. E.; Jahnke, F.; Koch, S. W. *Phys. Rev. Lett.* **1994**, *73*, 1785.
(37) Pompe, G.; Rappen, T.; Wegener, M. *Phys. Rev. B* **1995**, *51*, 7005.
(38) Arnaud, J. *Opt. Quantum Electron.* **1996**, *28*, 1589.
(39) Johnson, J. C.; Yan, H.; Yang, P.; Saykally, R. J. *J. Phys. Chem. B* **2003**, *107*, 8816.
(40) Soref, R. A. *IEEE J. Quantum Electron.* **1987**, *QE-23*, 123−129.
(41) Roxlo, C. B.; Putnam, R. S.; Salour, M. M. *IEEE J. Quantum Electron.* **1982**, *QE-18*, 338−342.
(42) Cho, C.-H.; Aspetti, C. O.; Turk, M. E.; Kikkawa, J. M.; Nam, S.-W.; Agarwal, R. *Nat. Mater.* **2011**, *10*, 669−675.